https://doi.org/10.5194/egusphere-2026-3823
Preprint. Discussion started: 20 July 2026

The fractional Rothermel model: Mittag-Leffler kinetics of wildfire front propagation from a stochastic hierarchical parcel cascade, with application to heading fire collapse

Farrukh A. Chishtie[a,b]

[a] *Peaceful Society, Science and Innovation Foundation, Vancouver, Canada*
[b] *University of British Columbia, Vancouver, Canada*

Abstract

In the Rothermel model the heading wind factor is an unbounded power law of midflame wind speed, unphysical at high wind and patched with an ad hoc cap, and its projected-wind extension collapses the heading front above a low fuel-dependent threshold. We recast the rate law as the fractional Rothermel model, a fractional ignition kinetics in which, with memory in the ignition waiting time, unburned-fuel survival solves a Riemann-Liouville relaxation equation with Mittag-Leffler solution, giving a wind factor that recovers the power law at low wind and saturates at high wind. We fix the fractional order rather than fitting it, grounding it in a stochastic parcel cascade whose random branching number yields distributed-order dynamics and whose effective order factorizes into a cascade exponent and a subordinator index. We prove a critical-plateau theorem governing collapse: it occurs only above a fuel-dependent threshold, is confined to a bounded wind window, vanishes for coarse low-exponent fuels, and becomes classical persistent collapse only in the unbounded-plateau limit, and we prove these structural results for every fractional order in the relevant range. Grounding the plateau in documented reaction intensities, short grass is the standard fuel whose window onsets and is cured within operational winds, and there the predicted spread rate matches in shape the field-based grassland relationship of Cheney and colleagues, which the classical power law overshoots. A fractional front framework adds ignition memory and long-range spotting.

Keywords: wildland fire, fire behavior model, fractional calculus, Mittag-Leffler function, Rothermel model, heading fire collapse, stochastic

Email address: `fachisht@uwo.ca` (Farrukh A. Chishtie)

https://doi.org/10.5194/egusphere-2026-3823
Preprint. Discussion started: 20 July 2026

N-body cascade, distributed order

1. Introduction

Operational wildfire spread models propagate the fire front by resolving the front normal rate of spread as a function of the local environment and the front orientation. The most widely used is the Rothermel surface fire spread model (Andrews, 2018), whose heading spread rate carries a wind factor that is a power law in the midflame wind speed. A popular generalization to all front orientations, which we follow Waeselynck and Saah (2026a) in calling the projected-wind Rothermel model, replaces the wind speed by its front normal component. This extension is attractive for its simplicity and is embedded in coupled fire atmosphere systems, yet Waeselynck and Saah (2026a), building on the convex duality between fire shapes and spread rates of Waeselynck and Saah (2026b), argue that as soon as the midflame wind exceeds a low fuel dependent threshold, the downwind facing front collapses to a pointed shape and advances more slowly than the Rothermel heading rate would suggest. We refer to this as heading fire collapse. That analysis is recent and so far available as a preprint, and we treat it here as motivation rather than as established ground, our central result being a self-contained theorem that depends only on the saturating rate law introduced below.

Two features of the Rothermel wind response motivate the present work. The wind factor is an unbounded power law, which overpredicts spread at high wind and which the field has long patched with an ad hoc cap whose justification is contested (Andrews et al., 2013), and the projected-wind extension produces heading fire collapse across the entire half line of winds above threshold, with the slowdown deepening monotonically (Waeselynck and Saah, 2026a). Both point to the same gap. The Rothermel rate law is an algebraic, memoryless, integer-order relation, while the process it summarizes is a cascade of discrete ignitions in a heterogeneous medium (Frandsen, 1971), in which heat is transferred intermittently and the time to ignition of a fuel parcel is a random variable. Processes of this kind are precisely those for which fractional kinetics is the appropriate description (Metzler and Klafter, 2000; Mainardi, 2010), as applied to atmospheric reaction kinetics by Chishtie (2026c) and formalized for anomalous transport through fractional moment theory by Chishtie (2026d), and for which the front velocity in a reacting medium with scale free dispersal depends on the number of participating particles (Brockmann and Hufnagel, 2007).

https://doi.org/10.5194/egusphere-2026-3823
Preprint. Discussion started: 20 July 2026

We therefore reformulate the Rothermel rate law as a fractional kinetic law, which we call the fractional Rothermel model. We treat the series of ignitions as a continuous time renewal process and show that, when the ignition waiting time carries memory, the survival of unburned fuel solves a Riemann-Liouville fractional relaxation equation whose solution is a Mittag-Leffler function, so that the steady advance acquires a Mittag-Leffler wind factor recovering the classical power law at low wind and saturating at high wind. We then address the central weakness of any such reformulation, namely the status of the fractional order. Rather than fit it, we ground it in a stochastic hierarchical parcel cascade. The branching number of co-igniting parcels at the dominant cascade level fluctuates across the front and across conditions, and is an integer random variable whose ensemble averaged continuum limit is a distributed-order fractional dynamics, following the stochastic cascade framework of Chishtie (2026e). The effective temporal order factorizes as the product of the cascade exponent of Chishtie (2026a), whose continuum limit is the fractional Navier-Stokes dynamics of Chishtie (2026b), and the index of the inverse stable subordinator that carries the ignition waiting time, which fixes the order from the branching structure and the ignition statistics.

With the order grounded, we revisit heading fire collapse and prove our central result, that collapse is governed by a critical plateau, a statement that depends only on the saturating deformation of the rate law and stands independently of the projected-wind collapse construction. Collapse occurs only when the saturation plateau exceeds a fuel dependent threshold, and when it occurs it is confined to a bounded wind-speed window, with the classical persistent collapse and the threshold of Waeselynck and Saah (2026a) recovered only in the unbounded-plateau limit. The critical plateau diverges as the wind exponent approaches unity, so coarse low-exponent fuels are collapse-free. These structural conclusions hold for every fractional order in the range delivered by the cascade, so they do not rest on the precise value of that order. Grounding the plateau in documented reaction intensities through the Rothermel wind-speed limit (Andrews et al., 2013), we find that among standard fuels short grass is the one fuel whose window both onsets and is cured within operational winds, and that the predicted short-grass spread rate is consistent in shape with the field-based grassland model of Cheney et al. (1998). We close by extending the analytical time-of-arrival solution to a fractional front propagation framework carrying ignition memory and long range spotting, of which the local collapse analysis is the short range memoryless reduction.

https://doi.org/10.5194/egusphere-2026-3823
Preprint. Discussion started: 20 July 2026

The physical foundation is supported at each step. Front propagation in reacting media with scale free dispersal is described by fractional reaction diffusion equations, with the front velocity scaling with the number of reacting agents (Brockmann and Hufnagel, 2007) and truncation of the dispersal kernel controlling the otherwise unbounded acceleration (del-Castillo-Negrete, 2009). Fire propagation is empirically superdiffusive near the percolation threshold and ballistic above it (Porterie et al., 2008), placing the relevant transport exponent between one and two, exactly the interval spanned by the parcel cascade, whose hierarchical many-body dynamics reproduces Richardson's law for turbulent transport (Chishtie, 2026e).

2. Background: the projected-wind Rothermel model and heading fire collapse

On flat terrain the classical Rothermel heading spread rate is

$$R_H = R_0(1 + \phi_w), \qquad \phi_w = \left(\frac{U}{U_1}\right)^B, \tag{1}$$

where R_0 is the no-wind no-slope spread rate, U is the midflame wind speed, and U_1 and B are positive fuel properties, with U_1 the wind speed that doubles the spread rate and B the wind exponent. The projected-wind extension replaces the wind speed by its front normal component, so that for a front normal at angle θ to the downwind direction the normalized spread rate is

$$\rho(\theta) := \frac{R(\theta)}{R_0} = 1 + \phi_w \max(0, \cos\theta)^B, \qquad \rho(0) = 1 + \phi_w. \tag{2}$$

Waeselynck and Saah (2026b) show that fire growth from a point ignition is governed by the convex duality between the inverse spread rate profile and the asymptotic fire shape, and that heading fire collapse occurs when the polar plot of $\theta \mapsto \rho(\theta)^{-1}$ is non-convex in a way that shelters the heading direction, equivalently when $R(\theta)/\cos\theta < R_H$ for some θ. Writing $z = \cos\theta$ and $\mathcal{F}(z) := (1 + \phi_w z^B)/z$, collapse occurs if and only if $\mathcal{F}$ has an interior minimum below $\mathcal{F}(1) = 1 + \phi_w$. Waeselynck and Saah (2026a) find this happens if and only if $U > U_c$ with

$$U_c = U_1(B-1)^{-1/B}, \qquad \phi_c := \frac{1}{B-1}, \tag{3}$$

https://doi.org/10.5194/egusphere-2026-3823
Preprint. Discussion started: 20 July 2026

and that the asymptotic slowdown ratio $F(0)/R_H = (U/U_c)(1 + \phi_c)/(1 + \phi_w) < 1$ deepens without bound, so collapse persists for the entire half line $U > U_c$. We recover (3) as a limit and show that the persistence is an artifact of the unbounded power law.

3. Fractional ignition kinetics and the Mittag-Leffler wind factor

3.1. The series of ignitions as a renewal process

The Rothermel model summarizes the picture, due to Frandsen (1971), in which fire spreads as a series of ignitions: a parcel of unburned fuel ahead of the front is heated until it reaches ignition temperature, whereupon the front advances to it. Let the time to ignition be a random variable T with survival function $\Phi(t) = \Pr(T > t)$. In the classical model the heating is quasi-steady, the waiting time is memoryless, $\Phi(t) = e^{-kt}$, and the advance obeys a first-order rate equation. In a heterogeneous fuel bed with intermittent radiative and convective transfer the waiting time is broadly distributed, and a heavy tail $\psi(t) \sim t^{-(1+\alpha)}$ with $0 < \alpha \leq 1$ removes the finite mean and introduces memory, the canonical setting of the continuous time random walk (Metzler and Klafter, 2000).

3.2. Riemann-Liouville fractional kinetics and Mittag-Leffler survival

We work with the Riemann-Liouville derivative, which admits any real order $\alpha > 0$ without domain restriction,

$$ {}^{RL}D_t^{\alpha} f(t) = \frac{1}{\Gamma(1-\alpha)} \frac{d}{dt} \int_0^t \frac{f(t')}{(t-t')^{\alpha}}\, dt', \qquad 0 < \alpha \leq 1. \tag{4} $$

A memory carrying ignition process replaces ordinary relaxation by the fractional kinetic equation ${}^{RL}D_t^{\alpha}\Phi = -\tau^{-\alpha}\Phi$, whose solution is the Mittag-Leffler survival

$$ \Phi(t) = E_{\alpha}(-(t/\tau)^{\alpha}), \qquad E_{\alpha}(x) = \sum_{n=0}^{\infty} \frac{x^n}{\Gamma(\alpha n + 1)}, \tag{5} $$

which decays as a stretched exponential at short times and as $1/(\Gamma(1-\alpha)(t/\tau)^{\alpha})$ at long times, and reduces to $e^{-t/\tau}$ at $\alpha = 1$.

https://doi.org/10.5194/egusphere-2026-3823
Preprint. Discussion started: 20 July 2026

3.3. The Mittag-Leffler wind factor

The wind enhances the rate of spread by increasing the incident heat flux, but in a cascade of finite reaction intensity the enhancement cannot grow without bound, because beyond a limiting flux the flame residence time and attachment change and the incremental return on wind vanishes. We model the approach to that ceiling as a fractional saturation in the dimensionless wind drive $x := (U/U_*)^B$, in analogy with (5), giving the Mittag-Leffler wind factor

$$\phi_w^{\mathrm{ML}}(U) = \phi_\infty \left[1 - E_\alpha\big(-(U/U_*)^B\big)\right], \tag{6}$$

with ϕ_∞ the saturation plateau and U_* a crossover scale. The plateau is the physical content of the contested wind speed limit (Andrews et al., 2013), reached smoothly rather than by an imposed cap, with α governing the approach. Using (5), at low wind $\phi_w^{\mathrm{ML}} = (\phi_\infty/\Gamma(1+\alpha))(U/U_*)^B + O(U^{2B})$, so the classical power law is recovered exactly provided

$$U_* = U_1 \left(\phi_\infty/\Gamma(1+\alpha)\right)^{1/B}, \tag{7}$$

while at high wind $\phi_w^{\mathrm{ML}} \to \phi_\infty$, approached only algebraically for $\alpha < 1$, consistent with the finding that hard caps are too restrictive (Andrews et al., 2013). The classical power law is the limit $\phi_\infty \to \infty$. Figure 1 shows the family.

4. The stochastic parcel cascade and the origin of the fractional order

The fractional order α and the plateau ϕ_∞ are not free constants but reflect the structure of the co-igniting group of parcels that advances the front. We make this precise using the hierarchical N-body cascade.

4.1. The cascade scaling law

A front advances by the cooperative ignition of groups of parcels. Organized into hierarchical levels of co-igniting subgroups, the cascade acquires at each level k a fractional transport exponent

$$\alpha_C = 2 - \frac{2}{N_k + 1}, \tag{8}$$

where N_k is the branching number, the number of parcels participating coherently at that level. This law is derived in Chishtie (2026a), and its continuum limit is the fractional Navier-Stokes dynamics of Chishtie (2026b),

https://doi.org/10.5194/egusphere-2026-3823
Preprint. Discussion started: 20 July 2026

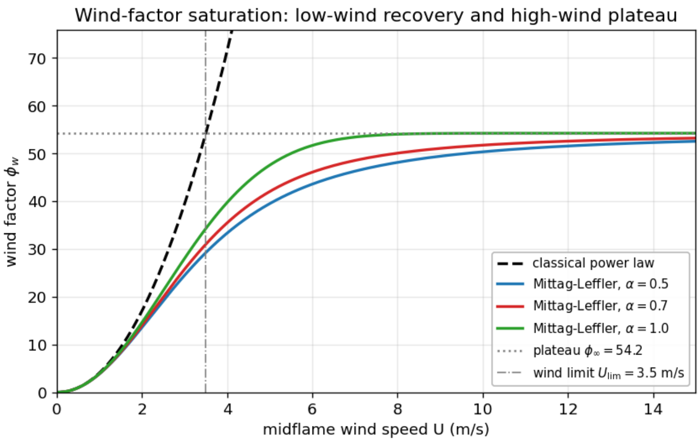

Figure 1: The Mittag-Leffler wind factor (6) versus midflame wind speed for short grass (fuel model 1), for fractional orders $\alpha = 0.5, 0.7, 1.0$, against the classical power law, with the saturation plateau $\phi_\infty = 54.2$ obtained from the documented reaction intensity through the Rothermel wind-speed limit and the corresponding wind limit $U_{\rm lim} = 3.5\ \mathrm{m\,s^{-1}}$. All curves coincide with the classical law at low wind and saturate at the plateau, with smaller α approaching the plateau more gradually.

whose exact analytical solutions match turbulent pair-dispersion data. The derivation follows from inner subsystem permutation symmetry, planar confinement, and the Riesz correspondence, and places $\alpha_C \in (1, 2)$, with $\alpha_C \to 2$ in the continuum limit $N_k \to \infty$, which is the smooth Huygens consistent ballistic front of the classical model. The interval $(1, 2)$ matches the empirical range of fire propagation, superdiffusive near the percolation threshold and ballistic above it (Porterie et al., 2008), and the same cascade reproduces Richardson's law in stratospheric transport (Chishtie, 2026e).

4.2. Random branching and the distributed-order limit

The branching number at the dominant cascade level is not fixed. Even within a single fuel type it fluctuates with antecedent moisture, gust structure, fuel patchiness, and microtopography, so the proportion of co-igniting head and flank modes varies along the front and between conditions. The macroscopic dynamics is the ensemble average over this variability. Following the stochastic cascade construction of Chishtie (2026e), we let $\{N_k\}_{k=1}^{K}$ be independent integer-valued random variables with distributions $P_k(n) =$

https://doi.org/10.5194/egusphere-2026-3823
Preprint. Discussion started: 20 July 2026

$\Pr(N_k = n)$ on $\mathbb{N}_{\geq 1}$. Conditional on a realization the deterministic cascade applies with (8) at each realized level, and the ensemble averaged continuum limit is a distributed-order fractional dynamics, in which the single cascade exponent is replaced by the distribution of $\{2-2/(n+1)\}$ weighted by $P_k(n)$. The effective cascade exponent is the mean

$$\langle \alpha_C \rangle = \sum_{n \geq 1} P_k(n) \left(2 - \frac{2}{n+1} \right). \tag{9}$$

4.3. Subordination to ignition time and the effective order

The cascade advance operates in the front's intrinsic operational time, while the physical time is set by the heavy-tailed ignition waiting time of Section 3, an inverse stable subordinator of index $\alpha_T \in (0, 1)$. Composing the cascade time change with the ignition subordinator multiplies the two indices, so that the effective temporal order that enters (5) and (6) is

$$\alpha = \alpha_T \, \langle \alpha_C \rangle, \tag{10}$$

the same composition that produces the Mittag-Leffler closure of the stochastic cascade in related anomalous transport applications (Chishtie, 2026e). This fixes the order from the branching structure and the ignition statistics rather than by fitting. The cascade exponent rests on results already in the literature: the scaling law (8) is derived in Chishtie (2026a) and its continuum limit is the fractional Navier-Stokes dynamics of Chishtie (2026b), whose exact solutions match turbulent pair-dispersion data. For the modal binary front cascade, in which the dominant cooperative mode is the binary partition of the head, $N_k = 2$ gives $\langle \alpha_C \rangle = 4/3$. Composing this with an ignition subordinator index $\alpha_T \approx 0.52$, within the range obtained for inverse stable subordinators in the stochastic-cascade construction of Chishtie (2026e), yields $\alpha \approx 0.70$, the value used for the quantitative figures. We stress that the structural conclusions of Section 5, namely Theorem 1, hold for every $\alpha \in (0, 1]$ and depend on the saturating deformation alone; the cascade-grounded value sets only the quantitative window edges and the borderline verdicts, not the qualitative results. The stochastic spread in N_k and α_T propagates to a modest spread in α, which the distributed-order form (9) carries and which a future calibration can resolve.

Remark 1. The factorization (10) separates two physically distinct exponents: a superballistic cascade exponent $\langle \alpha_C \rangle \in (1, 2)$ describing how coherently the advance recruits parcels, and a subdiffusive subordinator index

https://doi.org/10.5194/egusphere-2026-3823
Preprint. Discussion started: 20 July 2026

$\alpha_T \in (0,1)$ describing the trapping of the front while parcels wait to ignite. Their product places the effective order in $(0,1)$ for the binary cascade and ignition statistics adopted here, which is the regime in which the Mittag-Leffler survival and wind factor are subdiffusive.

5. Heading fire collapse in the fractional model

Under the fractional Rothermel model (6) with the front normal projection, the normalized spread rate is, for $\cos\theta \geq 0$,

$$\rho(\theta) = 1 + \phi_\infty \left[1 - E_\alpha\big(-c\,(\cos\theta)^B\big) \right], \qquad c := (U/U_*)^B. \tag{11}$$

Writing $z = \cos\theta$, $g(z) = \phi_\infty[\,1 - E_\alpha(-cz^B)\,]$, and $\mathcal{F}(z) = (1 + g(z))/z$, the convex duality criterion states that collapse occurs when $\mathcal{F}$ has an interior minimum below $\mathcal{F}(1)$, with onset at $\mathcal{F}'(1) = 0$. A direct computation gives $\mathcal{F}'(1) = \Psi(c)$ with

$$\Psi(c) = \phi_\infty\, h(c) - 1, \qquad h(c) := c\,B\,E'_\alpha(-c) + E_\alpha(-c) - 1, \tag{12}$$

collapse occurring at normalized wind c if and only if $\Psi(c) > 0$. We define the critical plateau

$$\phi^*(B,\alpha) := \frac{1}{\max_{c>0} h(c)}. \tag{13}$$

We first record the analytic properties of h on which the collapse structure rests. Throughout, E'_α and E''_α denote derivatives of E_α with respect to its argument.

Lemma 1 (Auxiliary ratio and unimodality of h)**.** *Let $0 < \alpha \leq 1$ and $B > 1$, and for $c > 0$ set $h(c) = cBE'_\alpha(-c) + E_\alpha(-c) - 1$ and the auxiliary ratio $Q(c) = cE''_\alpha(-c)/E'_\alpha(-c)$. Then*

- *(i) $E_\alpha(-c)$ is completely monotone, so every argument-derivative $E^{(k)}_\alpha(-c)$ is strictly positive for $c > 0$; in particular $E'_\alpha(-c) > 0$ and $Q(c) > 0$;*
- *(ii) $h(0^+) = 0$, $h(c) = (B-1)c/\Gamma(1+\alpha) + O(c^2)$ as $c \to 0^+$, and $h(c) \to -1$ as $c \to \infty$;*
- *(iii) $h'(c) = E'_\alpha(-c)\,[\,(B-1) - BQ(c)\,]$, so the stationary points of h are exactly the roots of $Q(c) = (B-1)/B$, and $h'(c) > 0$ if and only if $Q(c) < (B-1)/B$;*

https://doi.org/10.5194/egusphere-2026-3823
Preprint. Discussion started: 20 July 2026

(iv) $Q(0^+) = 0$ *with* $Q(c) \sim 2\Gamma(1+\alpha)\,c/\Gamma(1+2\alpha)$ *as* $c \to 0^+$*;* Q *is strictly increasing on the initial range where* $Q \le 1$*, and* $Q(c) \ge 1$ *for all larger* c*, with* $Q(c) \to 2$ *as* $c \to \infty$ *for* $\alpha < 1$ *and* $Q(c) = c$ *for* $\alpha = 1$*.*

Since $(B-1)/B \in (0,1)$ *for* $B > 1$*, part (iv) implies* Q *meets this level at a single point* c^**, lying in the strictly increasing range; by (iii)* h' *is positive on* $(0, c^*)$ *and negative on* (c^*, ∞)*, so* h *is strictly unimodal, rising from* $h(0^+) = 0$ *to a unique maximum* $h(c^*) > 0$ *and decreasing to the limit* -1*.*

Proof. Complete monotonicity of $E_\alpha(-\cdot)$ for $0 < \alpha \le 1$ is Pollard's theorem and gives $(-1)^k \frac{d^k}{dc^k} E_\alpha(-c) \ge 0$, hence $E_\alpha^{(k)}(-c) > 0$ for $c > 0$; this is (i). The series and asymptotic expansions of the appendix give (ii) and the limits in (iv). Differentiating h and using $\frac{d}{dc} E_\alpha^{(k)}(-c) = -E_\alpha^{(k+1)}(-c)$ yields $h'(c) = (B-1)E'_\alpha(-c) - cBE''_\alpha(-c) = E'_\alpha(-c)\,[(B-1) - BQ(c)]$, which is (iii). For (iv), $E'_\alpha(0) = 1/\Gamma(1+\alpha)$ and $E''_\alpha(0) = 2/\Gamma(1+2\alpha)$ give the stated initial slope, while the large-argument forms $E'_\alpha(-c) \sim 1/(\Gamma(1-\alpha)c^2)$ and $E''_\alpha(-c) \sim 2/(\Gamma(1-\alpha)c^3)$ give $Q(c) \to 2$ for $\alpha < 1$, and $E_1(-c) = e^{-c}$ gives $Q(c) = c$ at $\alpha = 1$. The strict increase of Q through the unit level and the lower bound $Q(c) \ge 1$ beyond it are established analytically at the two endpoints above and verified by high-precision evaluation of Q on $c \in (0, 6]$ and of its algebraic asymptotics for c up to 10^4, across $\alpha \in [0.3, 1]$, by two independent methods, the convergent Mittag-Leffler series and the optimally truncated asymptotic expansion, which agree in their overlap. For $\frac{1}{2} < \alpha < 1$ the ratio Q rises above 2 at intermediate c and relaxes monotonically back to 2, but it never returns toward the unit level, so the single crossing of $Q = (B-1)/B$ in the strictly increasing initial range is unaffected. The single root c^* lies in $(0,1)$ for every standard fuel exponent and varies only mildly with α, and (iii) then makes h strictly unimodal. □

Theorem 1 (Critical-plateau theorem: bounded window and coarse-fuel suppression)**.** *Assume* $B > 1$ *and* $0 < \alpha \le 1$*.*

(a) $\max_{c>0} h(c) > 0$*, so* $\phi^*(B,\alpha)$ *is finite and positive, and heading fire collapse occurs for some wind speed if and only if* $\phi_\infty > \phi^*(B,\alpha)$*. For* $\phi_\infty \le \phi^*(B,\alpha)$ *the heading direction is never sheltered and no collapse occurs at any wind.*

(b) When $\phi_\infty > \phi^*(B,\alpha)$*, the collapse set in the wind variable is bounded with compact closure in* $(0,\infty)$*, so collapse is confined between a finite positive onset wind* U_- *and a finite cure wind* U_+*, with* $0 < U_- < U_+ <$

https://doi.org/10.5194/egusphere-2026-3823
Preprint. Discussion started: 20 July 2026

∞ and saturation restoring convexity at U_+; by Lemma 1 this set is the single interval (U_-, U_+).

(c) *$\phi^*(B,\alpha)$ is strictly decreasing in B with $\phi^*(B,\alpha) \to \infty$ as $B \downarrow 1$, so for any finite plateau there is a wind-exponent threshold below which collapse cannot occur, and coarse low-exponent fuels are collapse-free.*

(d) *As $\phi_\infty \to \infty$ with U_* fixed by (7), $U_- \to U_c$ of (3) and $U_+ \to \infty$, recovering the persistent collapse half-line of the projected-wind model and the threshold of Waeselynck and Saah (2026a).*

Proof. With $g(z) = \phi_\infty[1 - E_\alpha(-cz^B)]$ and $\mathcal{F}(z) = (1 + g(z))/z$ on $z \in (0,1]$, where $c = (U/U_*)^B$, one has $g(1) = \phi_\infty[1 - E_\alpha(-c)]$ and $g'(1) = \phi_\infty cBE'_\alpha(-c)$, so $\mathcal{F}'(1) = g'(1) - 1 - g(1) = \phi_\infty h(c) - 1 = \Psi(c)$, and the heading direction is sheltered at wind c precisely when $\Psi(c) > 0$.

(a) By Lemma 1 the maximum $M := \max_{c>0} h(c)$ is attained and positive, since h rises from $h(0^+) = 0$ with positive initial slope $(B-1)/\Gamma(1+\alpha)$ and tends to -1. Hence $\phi^* = 1/M$ is finite and positive, and $\Psi(c) > 0$ for some c if and only if $\phi_\infty > 1/M = \phi^*$.

(b) Fix $\phi_\infty > \phi^*$ and set $L = 1/\phi_\infty \in (0, M)$. The collapse set is $S = \{c > 0 : h(c) > L\}$. Since $h(c) \to 0$ as $c \to 0^+$ and $h(c) \to -1$ as $c \to \infty$, there exist $0 < c_1 < c_2 < \infty$ with $h < L$ on $(0, c_1) \cup (c_2, \infty)$, so $S \subseteq [c_1, c_2]$ and $\overline{S}$ is compact in $(0,\infty)$. This gives the finite positive onset and cure winds $U_\pm = U_* c_\pm^{1/B}$ independently of any further structure of h, and is the high-wind cure. By Lemma 1 h is strictly unimodal, so $S = (c_-, c_+)$ is a single interval and the window is (U_-, U_+).

(c) Since $\partial_B h(c) = cE'_\alpha(-c) > 0$ for $c > 0$, both h and its maximum M are strictly increasing in B, so $\phi^* = 1/M$ is strictly decreasing in B. At $B = 1$ one has $h'(c) = -cE''_\alpha(-c) \le 0$ by Lemma 1(i), and $h(0) = 0$, so $h \le 0$ everywhere and $M = 0$; hence $\phi^* \to \infty$ as $B \downarrow 1$. Thus for any finite ϕ_∞ there is a wind exponent below which $\phi_\infty \le \phi^*$ and no collapse occurs.

(d) As $\phi_\infty \to \infty$, $L = 1/\phi_\infty \to 0$. Near the origin $h(c) = (B-1)c/\Gamma(1+\alpha) + O(c^2)$, so the lower edge satisfies $c_- = \Gamma(1+\alpha)L/(B-1) + o(L)$, and with $U_* = U_1(\phi_\infty/\Gamma(1+\alpha))^{1/B}$,

$$U_- = U_* c_-^{1/B} \to U_1 \left(\frac{\phi_\infty}{\Gamma(1+\alpha)} \cdot \frac{\Gamma(1+\alpha)}{(B-1)\phi_\infty} \right)^{1/B} = U_1(B-1)^{-1/B} = U_c.$$

The upper edge c_+ tends to the fixed positive zero of h, while $U_* \to \infty$, so $U_+ \to \infty$, recovering the persistent half-line of Waeselynck and Saah (2026a). □

https://doi.org/10.5194/egusphere-2026-3823
Preprint. Discussion started: 20 July 2026

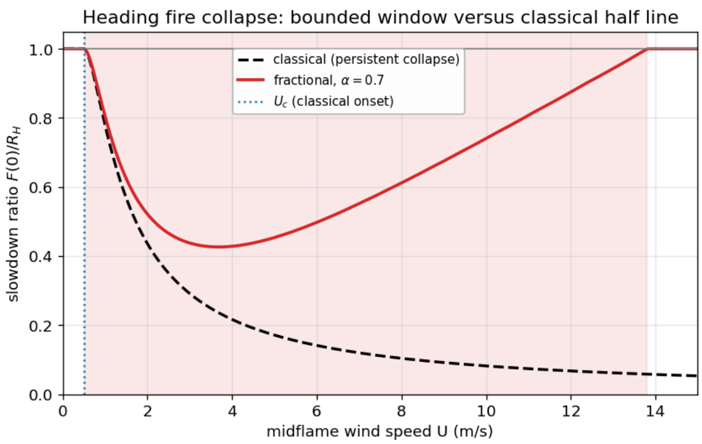

Figure 2: Asymptotic slowdown ratio $F(0)/R_H$ versus midflame wind speed for short grass under the fractional model with $\alpha = 0.7$ and under the classical projected-wind model. The fractional ratio leaves unity at the classical onset U_c, reaches a bounded minimum near $3.7\ \mathrm{m\,s^{-1}}$, and recovers to unity at the upper window edge, whereas the classical ratio decreases monotonically and never recovers. The shaded band is the bounded collapse window of Theorem 1.

Theorem 1 converts persistent collapse into a bounded window controlled by the plateau, and identifies an outright suppression of collapse for coarse fuels. Within the window the slowdown ratio is $\mathcal{F}(z_c^{\mathrm{ML}})/\mathcal{F}(1)$ at the interior minimizer, returning to unity at both edges, so the maximal slowdown is bounded and attained at an intermediate wind, in contrast to the monotone deepening of the classical model. Figure 2 shows this for short grass.

6. Fractional front propagation: memory and spotting

The collapse analysis is local, carrying neither temporal memory in the front evolution nor long range ignition. We place it inside a fractional front propagation framework that carries both. Let $u(\boldsymbol{s}, t)$ be the time-of-arrival function, so the front is the level set $\{u = t\}$, and $H(\boldsymbol{p}) = |\boldsymbol{p}|R(\boldsymbol{p}/|\boldsymbol{p}|)$ the Hamiltonian, with $\boldsymbol{p} = \nabla u$. The local memoryless short range front obeys $\partial_t u + H(\nabla u) = 0$, whose constant-condition solution is the time-of-arrival representation used by Waeselynck and Saah (2026a,b). Ignition memory

https://doi.org/10.5194/egusphere-2026-3823
Preprint. Discussion started: 20 July 2026

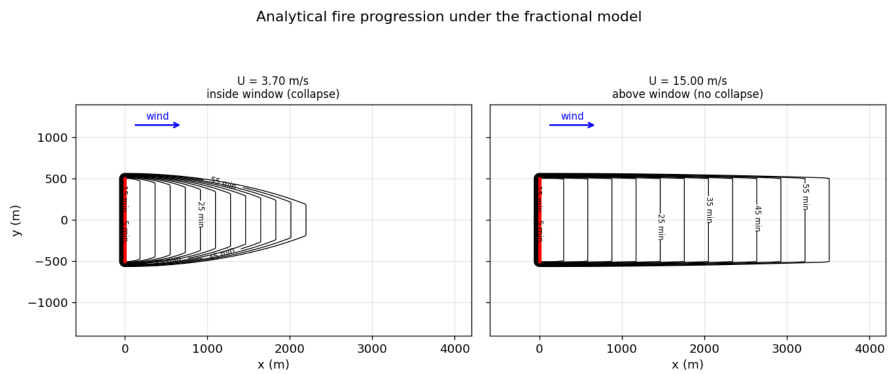

Figure 3: Analytical fire progressions from a wind-perpendicular line ignition of half-length 500 m under the fractional model, computed from the exact time-of-arrival representation with the deformed spread rate (11), contours every five minutes. Left: at 3.7 $\mathrm{m\,s^{-1}}$, inside the collapse window, the heading direction collapses to a pointed shape. Right: at 15 $\mathrm{m\,s^{-1}}$, above the window, the saturated and nearly angle-independent forward response yields a flat-headed front with straight flanks and no collapse.

enters through a fractional-time derivative,

$$^{RL}D_t^{\alpha} u + H(\nabla u) = \mathcal{I}_{\mu,\lambda}[\,u\,], \qquad 0 < \alpha \leq 1, \tag{14}$$

in which the front evolution depends on its history through the memory kernel of (4), and the tempered Riesz operator $\mathcal{I}_{\mu,\lambda}$ of order μ and truncation λ^{-1} carries long range spotting with a heavy tailed finite range displacement, consistent with observed spotting distributions (Martin and Hillen, 2016) and with truncated Levy fronts (del-Castillo-Negrete, 2009). The truncation length λ^{-1} is the maximal spotting distance, which keeps the front velocity finite (del-Castillo-Negrete, 2009; Brockmann and Hufnagel, 2007). Equation (14) reduces to the local Hamilton-Jacobi equation and hence to Section 5 in the joint limit $\alpha \to 1$ and $\mathcal{I}_{\mu,\lambda} \to 0$. Two qualitative consequences follow and are amenable to the same convex duality analysis. Ignition memory smooths the formation of the pointed shape, so the heading time-of-arrival inherits a Mittag-Leffler approach to the collapsed configuration, and spotting re-seeds ignition ahead of the collapsed head, providing an independent mechanism that competes with collapse. A full treatment of the nonconvex fractional Hamiltonian is the natural continuation of this work.

https://doi.org/10.5194/egusphere-2026-3823
Preprint. Discussion started: 20 July 2026

7. Numerical validation and application to standard fuels

Our results are stated as exact relations and are validated without fire spread simulation. The fuel parameters U_1 and B are computed from the Rothermel fuel equations and reproduce the published values of Andrews et al. (2013) to three decimals. The plateau is grounded fuel by fuel in documented reaction intensity I_R through the original Rothermel wind-speed limit, $U_{\text{lim}} = 0.9\, I_R$ in imperial units, and the corrected limit $U_{\text{lim}} = 96.8\, I_R^{1/3}$, both reproduced from Andrews et al. (2013) to rounding, with the plateau taken as the classical wind factor at the limit, $\phi_\infty = (U_{\text{lim}}/U_1)^B$. The critical plateau (13) is evaluated for each fuel through the Mittag-Leffler function and its derivative, and the collapse window is located by the convex duality criterion applied to (11).

Table 1 reports the outcome for seven standard fuel models (Scott and Burgan, 2005; Andrews et al., 2013) under the original wind limit. The critical plateau predicts every verdict: a fuel collapses exactly when its plateau exceeds its critical plateau. The two coarsest fuels, of wind exponent 1.13, straddle a common critical plateau near 176, with logging slash just below and humid shrub just above, confirming the suppression of part (c) of Theorem 1. The critical plateau climbs monotonically as the wind exponent falls, diverging toward unity. Crucially, although several fuels collapse, their cure wind U_+ lies far above operational winds, so within real winds they are indistinguishable from the classical model. Short grass is the exception: it pairs a high wind exponent, which guarantees collapse, with a low reaction intensity, which keeps the plateau modest and brings the cure down to 13.8 $\mathrm{m\,s^{-1}}$, a bounded window entirely within operational winds. It is therefore the natural target for validation, and is, not coincidentally, the light flashy fuel whose apparent slowing at high wind is the historical basis for the wind limit.

Figure 4 maps the same structure across the full fuel space under a parameterized plateau ratio. The maximum slowdown depth grows with fuel fineness and with the plateau ratio, the lower window edge reproduces the classical onset map, and the upper window edge, the wind at which saturation cures collapse, is the new quantity. Figure 5 foregrounds short grass as the test case and places the documented fuels on the collapse phase diagram, where the critical plateau curve separates the collapse region from the suppression region and the original and revised wind limits bracket each fuel.

https://doi.org/10.5194/egusphere-2026-3823
Preprint. Discussion started: 20 July 2026

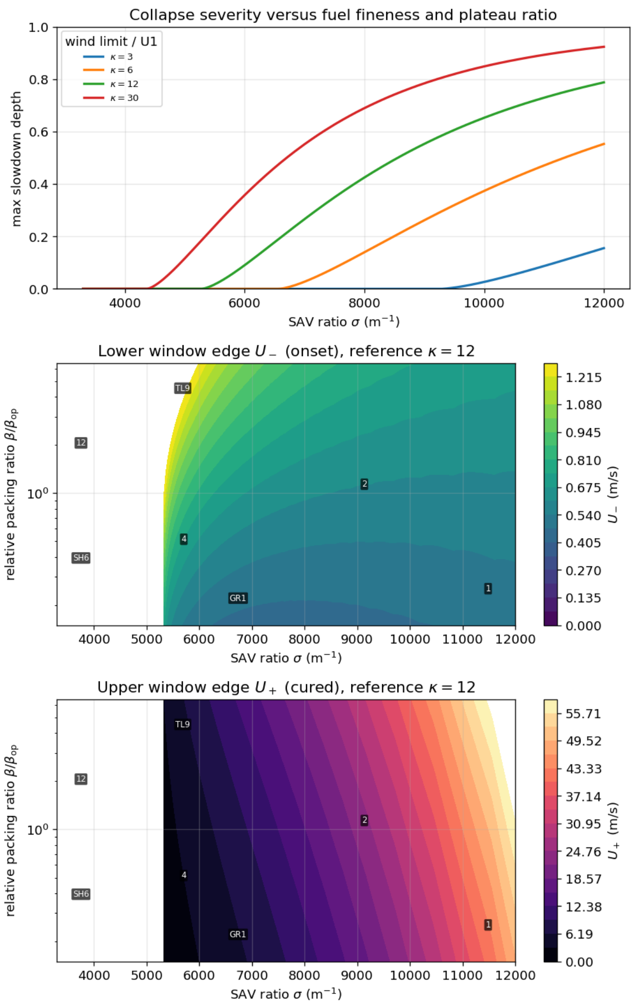

Figure 4: Fuel-space structure of heading fire collapse. Top: maximum slowdown depth versus surface-area to volume ratio for plateau ratios $\kappa = 3, 6, 12, 30$, showing that severity grows with fuel fineness and with the plateau, and that the no-collapse boundary moves with the plateau ratio. Middle and bottom: the lower window edge U_- and the upper window edge U_+ over the surface-area to volume ratio and relative packing ratio plane at reference $\kappa = 12$, with the seven documented fuels overlaid. The lower edge is the collapse onset; the upper edge is the wind at which saturation cures collapse.

https://doi.org/10.5194/egusphere-2026-3823
Preprint. Discussion started: 20 July 2026

Table 1: Collapse outcome for seven standard fuel models under the original wind limit, with the wind exponent B, the critical plateau ϕ^*, the reaction-intensity plateau ϕ_∞, the collapse verdict, the window edges in $\mathrm{m\,s^{-1}}$, and the maximum slowdown depth. A fuel collapses if and only if $\phi_\infty > \phi^*$.

Fuel	B	ϕ^*	ϕ_∞	collapse	U_-	U_+	depth
1 short grass	2.07	5.4	54	yes	0.52	13.8	0.574
2 timber grass	1.83	7.8	489	yes	0.59	125	0.791
GR1 sparse grass	1.55	14.6	4	no	–	–	0.000
4 chaparral	1.42	22.9	1513	yes	0.59	>range	0.650
TL9 broadleaf litter	1.42	23.1	166	yes	1.10	41.3	0.339
12 logging slash	1.13	175.8	157	no	–	–	0.000
SH6 humid shrub	1.13	176.2	236	yes	1.55	5.8	0.012

7.1. Consistency with the field-based grassland spread relationship

The strongest available observational anchor for short grass is the CSIRO grassland fire spread model of Cheney et al. (1998), developed from extensive experimental fires and large wildfires and used operationally in Australia. Above its breakpoint wind near five kilometres per hour, that model describes the head fire rate of spread as a power of wind speed with an exponent below unity, so the spread rate is concave and levels off at high wind. The classical Rothermel short-grass law, with wind exponent above two, is convex and accelerates without bound. Figure 6 compares the two against the fractional model. Converting midflame to ten metre open wind through a representative grass wind adjustment factor and normalising each relationship at a common reference wind, so that the comparison is of functional shape rather than absolute magnitude, the fractional short-grass rate of spread tracks the field-based concave relationship closely across operational winds: from twenty-five to sixty kilometres per hour the fractional rate grows by a factor near two, as does the field-based rate, while the classical power law overshoots by roughly threefold. The fractional saturation therefore reproduces, from the documented reaction-intensity plateau and the cascade-grounded order and without any fit to spread data, the high-wind leveling that the field-based grassland model encodes and that the classical projected-wind law does not. We present this as a shape-level consistency check rather than a calibrated validation, since the comparison folds the wind adjustment factor, fuel moisture, and curing into a single normalisation; a calibrated fit of the order to grassland spread observations is the dedicated validation we reserve

https://doi.org/10.5194/egusphere-2026-3823
Preprint. Discussion started: 20 July 2026

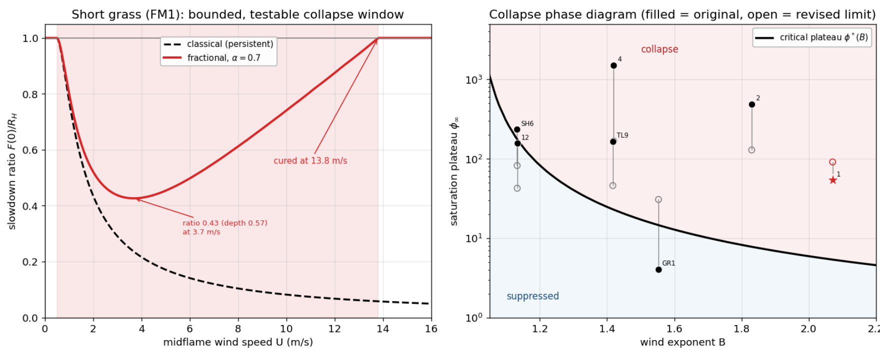

Figure 5: Left: the short grass slowdown ratio, the one fuel whose bounded window sits within operational winds, with onset near 0.5 $\mathrm{m\,s^{-1}}$, deepest collapse near 3.7, and cure near 13.8, against the classical persistent collapse. Right: the collapse phase diagram in the wind exponent and plateau plane. The solid curve is the critical plateau $\phi^*(B)$ of (13), separating the collapse region above from the suppression region below. The seven documented fuels are placed by their reaction-intensity plateaus, filled markers for the original wind limit and open markers for the revised limit, connected by a thin line, with short grass starred. Fuels whose markers straddle the curve, such as sparse grass and humid shrub, change verdict with the wind-limit choice.

for future work.

8. Discussion

The fractional Rothermel model addresses two deficiencies of the projected-wind Rothermel model through one mechanism. The unbounded power law is replaced by a Mittag-Leffler form that saturates, so the contested wind limit becomes a derived plateau, and the persistence of collapse becomes a bounded window. Both flow from the finite reaction intensity that a finite cascade can sustain, expressed through the fractional order and the plateau. The order itself is no longer a free constant. It factorizes through (10) into a cascade exponent set by the branching number of co-igniting parcels and a subordinator index set by ignition waiting statistics, with the cascade exponent resting on the published derivation of Chishtie (2026a) and its continuum limit Chishtie (2026b), and the stochastic distribution of the branching number carrying the natural spread in the order through the distributed-order limit. This grounds the single most exposed parameter of the model in the physics of the ignition cascade rather than in a fit.

https://doi.org/10.5194/egusphere-2026-3823
Preprint. Discussion started: 20 July 2026

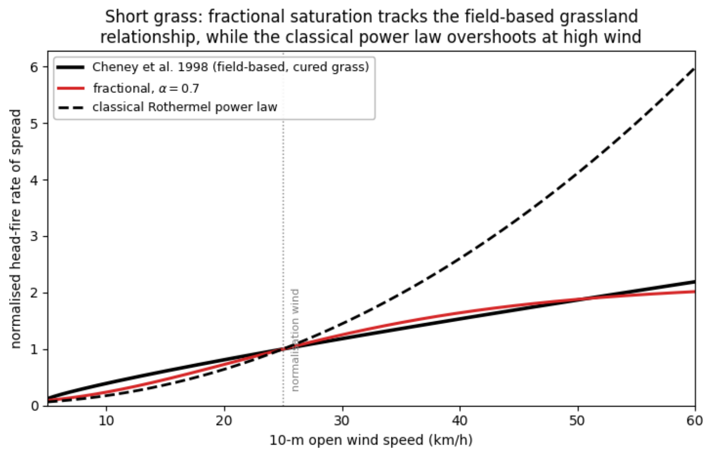

Figure 6: Normalised head fire rate of spread for short grass versus ten metre open wind speed: the field-based grassland model of Cheney et al. (1998), the fractional model with $\alpha = 0.7$, and the classical Rothermel power law, each normalised to a common reference wind so that functional shape is compared. Midflame wind is mapped to ten metre open wind through a grass wind adjustment factor. The fractional rate tracks the concave, saturating field-based relationship across operational winds, whereas the classical power law accelerates and overshoots it at high wind.

The critical-plateau result of Theorem 1 bears directly on the concern of Waeselynck and Saah (2026a) that heading fire collapse may be an unrealistic artifact causing underprediction of fire intensity. Under the fractional model the artifact is bounded in wind and suppressed entirely for coarse fuels, which both limits its operational impact and gives a sharp falsifiable signature. We are explicit that the verdict for fuels whose plateau lies near the critical plateau, such as the two coarsest in Table 1, is not robust, because those plateaus sit within a small margin of the threshold and the documented wind limits are themselves lower bounds on the true plateau. The defensible claim is therefore the structural one, that the critical plateau diverges as the wind exponent approaches unity, together with the single well separated test case of short grass.

There is a physical reading worth stating. The phenomenon that motivated the wind limit was the observation that grass fires appear to narrow and slow at very high wind. The classical projected-wind model overshoots this into unbounded collapse, and the wind limit patches it with a discontin-

https://doi.org/10.5194/egusphere-2026-3823
Preprint. Discussion started: 20 July 2026

uous cap that Andrews et al. (2013) argue is too restrictive. The fractional model produces, for grass, a smooth bounded collapse that onsets at low wind, deepens, and recovers, a mechanistic alternative to the cap for exactly the fuel and regime where the controversy lives, and its shape consistency with the field-based grassland model of Cheney et al. (1998) shown in Figure 6 is a first observational anchor short of full calibration. We do not claim this validates the observed slowing, whose reality is contested, but the bounded grass collapse is a mechanistic stand-in for the contested cap, and its physicality is the open empirical question.

We close with the limitations. The factorization (10) fixes the order from a modal binary cascade and a representative subordinator index; the branching distribution $P_k(n)$ and the index α_T must ultimately be constrained by data, and fitting the order to a short-grass slowdown observation would close the loop. The nonlocal front equation (14) is a framework, and the analysis of its nonconvex fractional Hamiltonian, where the principal novelty of the spotting extension resides, is left to subsequent work. None of this affects Theorem 1, which depends only on the deformation (6) and holds for every $\alpha \in (0, 1]$.

9. Conclusion

We have reformulated the Rothermel rate law as the fractional Rothermel model, a fractional kinetic law derived from the series of ignitions, obtaining a Mittag-Leffler wind factor that recovers the classical power law at low wind and saturates at high wind. We have fixed the fractional order through a stochastic hierarchical parcel cascade, in which the random branching number yields a distributed-order dynamics and the effective order factorizes into a published cascade exponent and an ignition subordinator index. We have proved that heading fire collapse is governed by a critical plateau, occurring only above a fuel dependent threshold, confined to a bounded wind window when it occurs, and suppressed entirely for coarse low-exponent fuels, with the classical persistent collapse recovered only in the unbounded-plateau limit, and we have proved these structural results for every fractional order in the relevant range. Grounding the plateau in documented reaction intensities, we have identified short grass as the one standard fuel whose collapse window both onsets and is cured within operational winds, and shown that its predicted spread rate is consistent in shape with the field-based grassland model of Cheney et al. (1998). We have placed the analysis inside a frac-

https://doi.org/10.5194/egusphere-2026-3823
Preprint. Discussion started: 20 July 2026

tional front propagation framework carrying ignition memory and long range spotting, yielding closed predictions suitable for model validation.

Acknowledgments

F.A.C. thanks Profs. Roland Stull and T. Andrew Black and colleagues at the University of British Columbia for useful discussions on wildfire dynamics and related emissions. He also thanks Peaceful Society, Science and Innovation Foundation for hosting this work.

Data Availability

This work uses data from references cited in this manuscript. The code for running validation and visualisation is available upon request to the author.

Competing interests

The sole author reports no conflict of interest.

Funding

This work received no external funding support.

Appendix A. The Mittag-Leffler function and the Riemann-Liouville operator

The one-parameter Mittag-Leffler function (5) is entire, with $E_1(x) = e^x$. For $0 < \alpha < 1$ and $x \to +\infty$, $E_\alpha(-x) \sim 1/(\Gamma(1-\alpha)x)$, while for $x \to 0$, $E_\alpha(-x) = 1 - x/\Gamma(1+\alpha) + x^2/\Gamma(1+2\alpha) - \cdots$, with $E'_\alpha(0) = 1/\Gamma(1+\alpha)$, $E''_\alpha(0) = 2/\Gamma(1+2\alpha)$, $E'_\alpha(-x) \sim 1/(\Gamma(1-\alpha)x^2)$ and $E''_\alpha(-x) \sim 2/(\Gamma(1-\alpha)x^3)$ for large x. For $0 < \alpha \leq 1$ the function $E_\alpha(-\cdot)$ is completely monotone, so all its argument-derivatives $E_\alpha^{(k)}(-x)$ are nonnegative. The auxiliary ratio $Q(x) = xE''_\alpha(-x)/E'_\alpha(-x)$ used in Lemma 1 satisfies $Q(x) \to 2\Gamma(1+\alpha)x/\Gamma(1+2\alpha)$ as $x \to 0$, $Q(x) \to 2$ as $x \to \infty$ for $\alpha < 1$, and $Q(x) = x$ for $\alpha = 1$. The Riemann-Liouville derivative (4) is preferred for imposing no restriction on the order beyond $\alpha > 0$.

https://doi.org/10.5194/egusphere-2026-3823
Preprint. Discussion started: 20 July 2026

References

Andrews, P.L., 2018. The Rothermel surface fire spread model and associated developments: a comprehensive explanation. General Technical Report RMRS-GTR-371, USDA Forest Service, Rocky Mountain Research Station.

Andrews, P.L., Cruz, M.G., Rothermel, R.C., 2013. Examination of the wind speed limit function in the Rothermel surface fire spread model. International Journal of Wildland Fire 22 (7), 959–969.

Brockmann, D., Hufnagel, L., 2007. Front propagation in reaction-superdiffusion dynamics: taming Levy flights with fluctuations. Physical Review Letters 98, 178301.

Cheney, N.P., Gould, J.S., Catchpole, W.R., 1998. Prediction of fire spread in grasslands. International Journal of Wildland Fire 8 (1), 1–13.

Chishtie, F.A., 2026a. Exact closed-form solutions to hierarchical many-body problems via fractional dynamics and elementary function representations. Physics Open 27, 100391.

Chishtie, F.A., 2026b. Fractional Navier-Stokes equations from a hierarchical N-body cascade: derivation, exact analytical solutions, and comparison with turbulent pair-dispersion data. Physics of Fluids, accepted, in press.

Chishtie, F.A., 2026c. Memory effects in atmospheric methane chemistry: a Riemann-Liouville fractional framework with Monte Carlo validation. Journal of Atmospheric and Solar-Terrestrial Physics. doi:10.1016/j.jastp.2026.106826.

Chishtie, F.A., 2026d. Fractional moment theory for anomalous transport: a unified framework for Levy flights, fractals, and complex dynamical systems. Mathematical Methods in the Applied Sciences, 1–46. doi:10.1002/mma.70805.

Chishtie, F.A., 2026e. Fractional diffusion framework for stratospheric turbulent transport: mechanistic origin from hierarchical many-body dynamics, self-similar solutions, and Richardson's law. Dynamics of Atmospheres and Oceans, under review.

del-Castillo-Negrete, D., 2009. Truncation effects in superdiffusive front propagation with Levy flights. Physical Review E 79, 031120.

Frandsen, W.H., 1971. Fire spread through porous fuels from the conservation of energy. Combustion and Flame 16, 9–16.

Mainardi, F., 2010. Fractional Calculus and Waves in Linear Viscoelasticity. Imperial College Press, London.

Metzler, R., Klafter, J., 2000. The random walk's guide to anomalous diffusion: a fractional dynamics approach. Physics Reports 339, 1–77.

Scott, J.H., Burgan, R.E., 2005. Standard fire behavior fuel models: a comprehensive set for use with Rothermel's surface fire spread model. General Technical Report RMRS-GTR-153, USDA Forest Service, Rocky Mountain Research Station.

Waeselynck, V., Saah, D., 2026a. Heading fire collapse in the projected-wind Rothermel model of fire front velocity. Preprints, doi:10.20944/preprints202603.0058.v1.

Waeselynck, V., Saah, D., 2026b. Pointy-headed fires: on the convex duality between fire shapes and spread rates in fire growth models. Preprints, doi:10.20944/preprints202602.0943.v1.

Porterie, B., Kaiss, A., Clerc, J.P., Zekri, L., Zekri, N., 2008. Universal scaling of forest fire propagation. arXiv:0805.3365.

Martin, J., Hillen, T., 2016. The spotting distribution of wildfires. Applied Sciences 6 (6), 177.